International Journal of Nanomedicine

Dovepress
open access to scientific and medical research

Open Access Full Text Article

ORIGINAL RESEARCH

Immunostimulatory Potential of MoS_2 Nanosheets: Enhancing Dendritic Cell Maturation, Migration and T Cell Elicitation

This article was published in the following Dove Press journal:
International Journal of Nanomedicine

Lei Deng[1,2]
Xiaoli Pan[1]
Yulong Zhang[1]
Sujing Sun[1]
Liping Lv[1]
Lei Gao[1]
Ping Ma[1]
Huisheng Ai[2]
Qianqian Zhou[1]
Xiaohui Wang[1]
Linsheng Zhan[1]

[1]Department of Emerging Transfusion Technology, Institute of Health Service and Transfusion Medicine, Academy of Military Medical Sciences, Beijing, People's Republic of China; [2]Department of Hematology, The Fifth Medical Center of Chinese PLA General Hospital, Beijing, People's Republic of China

Background: Due to their extraordinary physical and chemical properties, MoS_2 nanosheets (MSNs) are becoming more widely used in nanomedicine. However, their influence on immune systems remains unclear.

Materials and Methods: Two few-layered MSNs at sizes of 100–250 nm (S-MSNs) and 400–500 nm (L-MSNs) were used in this study. Bone marrow-derived dendritic cells (DCs) were exposed to both MSNs at different doses (0, 8, 16, 32, 64, 128 μg/mL) for 48 h and subjected to analyses of surface marker expression, cytokine secretion, lymphoid homing and in vivo T cell priming.

Results: Different-sized MSNs of all doses did not affect the viability of DCs. The expression of CD40, CD80, CD86 and CCR7 was significantly higher on both S-MSN- and L-MSN-treated DCs at a dose of 128 μg/mL. As the dose of MSN increased, the secretion of IL-12p70 remained unchanged, the secretion of IL-1β decreased, and the production of TNF-α increased. A significant increase in IL-6 was observed in the 128 μg/mL L-MSN-treated DCs. In particular, MSN treatment dramatically improved the ex vivo movement and in vivo homing ability of both the local resident and blood circulating DCs. Furthermore, the cytoskeleton rearrangement regulated by ROS elevation was responsible for the enhanced homing ability of the MSNs. More robust $CD4^+$ and $CD8^+$ T cell proliferation and activation (characterized by high expression of CD107a, CD69 and ICOS) was observed in mice vaccinated with MSN-treated DCs. Importantly, exposure to MSNs did not interrupt LPS-induced DC activation, homing and T cell priming.

Conclusion: Few-layered MSNs ranging from 100 to 500 nm in size could play an immunostimulatory role in enhancing DC maturation, migration and T cell elicitation, making them a good candidate for vaccine adjuvants. Investigation of this study will not only expand the applications of MSNs and other new transition metal dichalcogenides (TMDCs) but also shed light on the in vivo immune-risk evaluation of MSN-based nanomaterials.

Keywords: MoS_2 nanosheets, dendritic cells, migration, vaccine adjuvant

Correspondence: Xiaohui Wang; Linsheng Zhan
Department of Emerging Transfusion Technology, Institute of Health Service and Transfusion Medicine, Academy of Military Medical Sciences, Beijing, People's Republic of China
Email lszhan91@yahoo.com; lovechina1980@163.com

Introduction

As the most widely used two-dimensional (2D) nanomaterial, graphene has attracted the attention of biomedical researchers since it was first reported in 2004.[1] In recent years, transition metal dichalcogenides (TMDCs), another class of 2D nanomaterials, have emerged and have quickly become an active focus. Among them, mono or few-layer MoS_2 nanosheets (MSNs) have become a new favorite of nano-biologists. The high near

infrared ray absorbance, extraordinary electrocatalytic activity, easy surface modification and low biological toxicity make MSNs one of the most promising graphene analogues with wide applications in various fields, especially in nanobiomedicine.[2] To date, MSNs have been developed for use as bio-imaging probes,[3] biosensors,[4–6] photothermal therapy agents,[7–9] drug carriers[10–12] and tissue engineering scaffolds,[13] among other uses. The possibility of using MSNs as immune-regulatory adjuvants to manipulate the immune responses is also a very fascinating and a meaningful research topic. However, to the best of our knowledge, this application has yet to be studied. On the other hand, despite previous studies underlining the feasibility of employing MSNs as in vivo administered agents, the effect of these tissue-invasive foreign nanomaterials on the immune system remains to be revealed.

Dendritic cells (DCs), one of the most important antigen presenting cells, bridge the innate and adoptive immune response and have been proven to be associated with many serious diseases such as chronic infections, tumors and autoimmune disorders.[14,15] Considering the prominent role of DCs in the immune system, comprehensively exploring the mutual interaction between DCs and nanomaterials is critically important and constitutes an essential component of immune-risk evaluation. Most importantly, the maturing of the field of nanovaccinology demonstrated the unparalleled ability of nanomaterials to manipulate the immune system and thus generate controlled or broad-spectrum immune responses.[16–18] Focusing the effect of nanoparticles on DCs will also offer a myriad of opportunities for developing effective vaccine adjuvants.

DCs undergo two stages, ie, the immature stage and the mature stage, before presenting antigens to T cells. During the immature stage, DCs possess a high phagocytotic ability but low homing and T cell priming capacities.[19] When stimulated by pathogens or foreign invaders, immature DCs will transform into the mature stage, characterized by increased expression of co-stimulatory molecules (CD40, CD80 and CD86) and elevated proinflammatory cytokine secretion.[20,21] Under physiological conditions, invaded pathogens can efficiently activate tissue-resident DCs due to both the number of antigens they are exposed to as well as the accompanying strong stimulation from pathogen components (LPS, CpG, etc.), which exert their effects on the TLRs of DCs and promote the transition of DCs to the mature stage.[22] In contrast, in artificial immunity, generally only antigens are provided, leaving DCs in a state of semi-maturation. Although the semi-matured DCs are equipped with antigens, the lower expression of allostimulatory molecules and limited homing capability greatly hinders the T cell priming capacity.[23] Therefore, finding adjuvants capable of improving the maturation and migration abilities of DCs is key to optimizing traditional vaccination strategies.

In this study, we aimed to determine whether MSNs have immunoregulatory effects on DCs, focusing on the essential functional parameters of DCs (maturation, migration and T cell activation). MSNs of two sizes (100–250 nm for the smaller one and 400–500 nm for the larger one) were used in this study to clarify whether the size affects the outcomes. The dose effect was also taken into the consideration. To our knowledge, this is the first work to systematically explore the immunoregulatory role of MSNs. Our findings will provide supporting evidence as to the feasibility of using MSNs as a novel vaccination adjuvant, which will expand the applications of MSNs and other new TMDCs. This study will also shed light on the in vivo immune-risk evaluation of MSN-based nanomaterials.

Materials and Methods

Mice

Male wild-type C57BL/6J mice, 6–8 weeks old, were purchased from Beijing Vital River Laboratory Animal Technology Co., Ltd. C57BL/6J mice expressing GFP were purchased from the Model Animal Research Center of Nanjing University. LTD.L2G85 (FVB) mice expressing firefly luciferase (Fluc) were backcrossed into C57BL/6J mice and used in phase N7 (L2G85.C57BL/6). All experiments were approved by the committee on animal care and use of the Academy of Military Medical Sciences (Approval No.: AMMS-09-2019-004). All animal experiments followed the National Institutes of Health Guide for the Care and Use of Laboratory Animals.

Reagents and Antibodies

GM-CSF and IL-4 were purchased from Peprotech Asia (Rehovot, Israel). Lipopolysaccharide (LPS) and D-luciferin were purchased from Sigma Aldrich (Missouri, USA) and Promega Corporation (Madison, WI, USA), respectively. The following antibodies were used for FACS analysis: fluorescein isothiocyanate (FITC)-conjugated anti-CD80, FITC-conjugated anti-CD8α, phycoerythrin (PE)-conjugated anti-CCR7, PE-conjugated anti-CD107a, PE-conjugated anti-CD40, PE-conjugated anti-IFN-γ, allophycocyanin (APC)-conjugated anti-CD11c, APC-conjugated anti-CD3ε, APC-conjugated anti-TNF-α, APC-conjugated anti-CD69, allophycocyanin-cyanine (APC-cy7)-conjugated anti-CD45, APC-cy7-conjugated anti-ICOS, phycoerythrin-cyanine dye (PE-cy7)-conjugated anti-B220, PE-cy7-conjugated anti-CD86 and PerCP/

Cyanine5.5-conjugated anti-CD4. All FACS antibodies were purchased from BioLegend (San Diego, CA, USA).

Characterization of MSNs

MSNs of two sizes were purchased from Nanjing Xianfeng Nanometer Company (Jiangsu, China). The dispersed solvent was water at a concentration of 1 mg/mL. The sizes were 100–250 nm (S-MSNs) and 400–500 nm (L-MSNs). A drop of diluted particle solution was placed on a carbon-coated copper grid and dried over-night before observation. The size was characterized by atomic force microscopy and transmission electron microscopy (TEM, Hitachi H-7650, Japan) at the working voltage of 80 kV. The colloid stability in water and 1640 medium was tested by the Zetasizer Nano ZS90 system (Malvern Instruments, England).

Production of Dendritic Cells from Bone Marrow in Mice

After euthanasia, the femurs of C57BL/6J mice were collected. The femur bone marrow monocytes were cultured in RPMI-1640 medium (Life Technologies Corporation, California, USA) containing 10% fetal bovine serum (PAN-Biotech, Aidenbach, Germany), 10 ng/mL recombinant mouse GM-CSF and 5 ng/mL recombinant mouse IL-4 at a density of 2×10^6 cells. At days 3 and 5, we replaced the old medium with 2 mL fresh medium containing GM-CSF and IL-4. Cells cultured on day 6 were used as immature DCs.

MSNs-DC ex vivo Coincubation

For the MSN-DC incubation experiments, 1×10^6 DCs in 2 mL of complete RPMI 1640 were incubated with S-MSNs or L-MSNs at different concentrations for 48 h in six-well plates. N-acetyl-L-cysteine (NAC, Sigma, CA) was alternatively added to the MSN-DC incubation medium at a final concentration of 10 mM. For the lipopolysaccharide (LPS) incubation experiments, LPS (Sigma, CA) was alternatively added to the MSN-DC incubation medium at the final concentration of 1μg/mL. After 48 hours of coincubation, the cells were centrifuged at 400 g and washed in PBS. Then the cells were fixed with 2.5% glutaraldehyde (Sigma, CA) for 30 min, washed with PBS for 3 times, and fixed with 1% osmic acid (Merck, Schwalbach, Germany) for 30min. The cells were dehydrated with a gradient of ethanol concentration. After dehydrated by epoxy resin (Sigma, CA), the cells were dried in the embedded template of porous rubber and then sliced. Finally, DC cell phagocytosis was observed by transmission electron microscopy at the working voltage of 80 kV.

DC Phenotype and Apoptosis Detection

DCs were washed twice with cold PBS and then re-suspended in cell staining buffer. Corresponding antibodies were added to the cell suspension and then incubated at room temperature for 15 min. Cells were then washed twice with cold PBS for flow cytometry analysis. In apoptosis assay, cells were re-suspended in a binding buffer after staining with APC-anti-CD11c antibody. Annexin V-FITC and propidium iodide were added, incubated at 4°C for 30min, and then 300ul binding buffer was added for flow cytometry analysis.

Detection of Cytokine Secreted by DCs

The co-culture supernatants were collected by centrifuging at 400 g/min for 6 min. IL-6, IL-12p70, IL-1β and TNF-α were tested according to the instructions of the ELISA kit (Dakewe, Shenzhen, China).

In vitro Cellular Movement Analysis

DCs derived from GFP transgenic mice were monitored in a live cell imaging system (PerkinElmer, Massachusetts, USA), and time-lapse micrographs were tracked and analyzed using Volocity Demo software. The generated tracking data were used to plot the cell track and calculate the movement data.

Homing Ability of DCs in vivo

To test the homing ability of DCs in draining lymph nodes, 1×10^6 DCs derived from $Fluc^+$ mice were injected subcutaneously into the footpad of mice. The migration and homing ability of the dendritic cells were detected by the IVIS Spectrum system (PerkinElmer). ROI analysis of the images and signal intensity was performed with Living Image 4.5.2 software. To detect the distribution of DCs in vivo, a total of 5×10^6 DCs were injected into the tail vein of mice and photographed at 2 h. After 48 h, the organs and tissues were separated and photographed on a dark background panel.

Immunofluorescence Staining and Confocal Microscopy

DCs cultured in glass bottom cell culture dishes (NEST, Jiangsu, China) were fixed with 4% paraformaldehyde (Merck, Schwalbach, Germany) for 1 h. Then, the cells were incubated with 1% Triton X-100 (Sigma, Missouri, USA) for 15 min. After washing three times, DCs were then incubated

with 300 μL anti-β-tubulin (10 μg/mL, Abcam, Cambridge, UK) at 4 °C for 12 h. The cells were incubated with rhodamine-conjugated phalloidin (50 μg/mL, Thermo Fisher, Massachusetts, USA) and 488-conjugated goat anti-rabbit IgG (2 μg/mL, Abcam, Cambridge, UK) for 60 min after washing. After washing, the cells were incubated with DAPI medium to stain the nuclei. Confocal laser-scanning microscopy (PerkinElmer, Massachusetts, USA) was used to view cells.

Determination of Reactive Oxygen Species in DCs

Reactive oxygen species (ROS) intensities were detected by a fluorescent probe 2, 7-dichlorofluorescein (DCFH-DA) kit. DCs were cultured in glass bottom cell culture dishes. DCFH-DA (5 mol/L, 500 μL/sample) was added and incubated in a cell incubator for 20 min. Then, the fluorescence of the DCs was detected after washing with PBS for 2–3 times.

Detection of T Cell Proliferation and Activation

To detect the activation of T cells in vivo, we injected 2×10^6 co-incubated DCs into the footpad of mice on day 1 and day 7. On day 14, the popliteal lymph nodes of mice were dissected and then filtered through a 200-mesh filter to obtain 1 mL of a single-cell suspension. The total number of cells in the suspension was calculated by a cell counter (Countstar, Shanghai, China). Subsequently, the cells were washed with PBS and then re-suspended in cell staining buffer. Corresponding marker antibodies were added to detect T cell activation by FACS analysis. For intracellular cytokine detection, cells were stained with FITC-anti-CD8α antibody and then re-suspended in a fixation/permeabilization solution (BD, New Jersey, USA). After incubation at 4 °C for 20 min, the cells were washed with perm/wash buffer and then labeled by APC-anti-TNF-α and PE-anti-IFN-γ antibodies for 30 min at 4 °C. Cells were washed twice with perm/wash buffer before being subjected to FACS analysis.

Statistical Analysis

Data were analyzed using GraphPad Software (Version 6, San Diego, CA). Dunnett's *t*-test was used to analyze the normally distributed data. Non-parametric testing was used to analyze the non-normally distributed data. $P < 0.05$ indicates a significant difference.

Results and Discussion

Characterization of MSNs and Their Uptake by DCs

Atomic force microscopy (AFM) and transmission electron microscopy (TEM) were used to observe the lateral sizes of the MSNs. Figure 1A shows the thickness of the MSNs was in the range of 1–2 nm, suggesting they probably were mainly two or three-layered nanomaterials. According to the TEM micrographs, the lateral sizes of the two materials were 100–250 nm for the S-MSNs and 400–500 nm for the L-MSNs (Figure 1B). The X-ray diffraction (XRD) pattern indicated that the nanosheets exhibited the typical crystal structure of MSNs (Figure 1C). For the S-MSNs and the L-MSNs, the Zeta potentials in water were −42.53 ± 2.23 mV and −42.43 ± 1.34 mV, respectively, while in 1640 medium, they were elevated to −9.79 ± 0.73 mV and −8.82 ± 0.65 mV (Table S1). The formation of the protein corona by adsorption of the protein components onto the surface of the MSNs might be responsible for the decreased absolute potential values in 1640 medium. In Figure 1D, we observed that the nanosheets could be swallowed by DCs and were mainly located in intracellular vesicles in the cytoplasm, suggesting a direct interaction between DCs and MSNs existed.

The Dose Effect of MSNs on DC Viability and Maturation

DCs were exposed to both sized MSNs at different doses (0, 8, 16, 32, 64, 128 μg/mL) for 48 h and subjected to apoptosis analysis by combined staining with Annexin-□ and PI (Figure 2A). For DCs from both S-MSNs and L-MSNs, the overall viability, as well as the apoptosis percentage, showed no significant differences between the lowest dose (8 μg/mL) and the highest dose (128 μg/mL) (Figure 2B), thus demonstrating the low direct cytotoxicity of MSNs.

Allostimulatory molecules on DCs are tightly related to T cell activation because they provide the costimulatory signal in the DC-T cell interaction system. Positive percentages of CD40, CD80 and CD86 before and after incubation with MSNs were detected by FACS (Figure S1). A similar tendency was observed among all detected markers on both S-MSNs and L-MSNs pulsed with DCs, that is, the lower dose (8–64 μg/mL) had no effect on their expression, but a significantly elevated level was observed when the dose was increased to 128 μg/mL (Figure 2C). In addition, the proportion of CD80 and CD86 in the L-MSN group was significantly higher than that in the S-MSN group at 128 μg/mL. The expression of CCR7, a critically important chemokine receptor for DC in vivo homing, was measured simultaneously. In the S-MSN group, 32 μg/mL

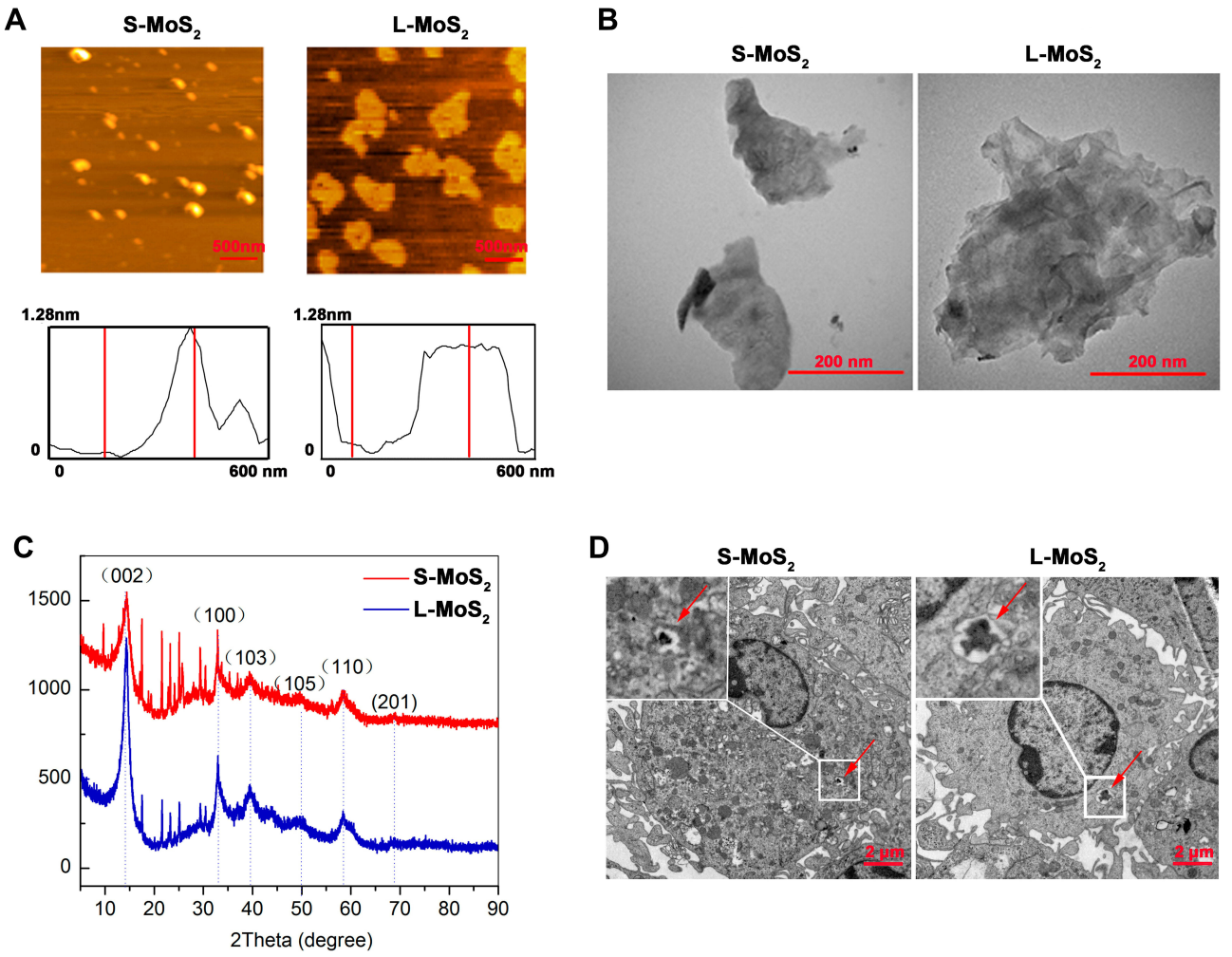

Figure 1 Characterization of the few-layered MSNs and their uptake by DCs.
Notes: (**A**) AFM images of MSNs. (**B**) TEM images of MSNs. (**C**) The XRD pattern of MSNs. (**D**) DCs were incubated with MSNs (128 μg/mL) for 48 h and observed by TEM to examine the cellular uptake of MSNs. The red arrow indicates the internalized MSNs.
Abbreviations: S-MoS_2, small MSNs; L-MoS_2, large MSNs; AFM, atomic force microscopy; XRD, X-ray diffraction; TEM, transmission electron microscopy; MSNs, MoS_2 nanosheets; DCs, dendritic cells.

was the lowest dose at which an obvious increase in CCR7 was observed. In comparison, no obvious changes were observed until the incubation dose was elevated to 128 μg/mL in the L-MSN group, suggesting that CCR7 is more sensitive to S-MSN treatment.

The secretion of proinflammatory cytokines also markedly change when DCs encounter an invading pathogen, which not only aids in T cell elicitation but also promotes DC maturation through a feedback mechanism. The concentration of IL-12p70, IL-6, IL-1β and TNF-α in the coincubation culture medium was measured (Figure 2D), and the results were inconsistent among them. The secretion of IL-12p70 remained unchanged at all evaluated doses in DCs treated with both S-MSNs and L-MSNs. TNF-α was significantly elevated at the lower incubation concentration (8 μg/mL) in both S-MSNs and L-MSNs. A significant increase in IL-6 was detected but only for DCs treated with 128 μg/mL L-MSNs. In contrast, IL-1β was obviously downregulated by both S-MSNs and L-MSNs at 64 μg/mL and 128 μg/mL, respectively.

In summary, the above results demonstrate that the direct cytotoxicity of MSNs was very weak, which is consistent with the findings of many previous reports using different cell lines and different MSN derivatives.[24–26] In addition, when incubated at a relatively higher dose (128 μg/mL), MSNs could promote DC maturation as characterized by upregulated expression of CD40, CD80 and CD86 and enhanced secretion of IL-6 and TNF-α. We speculate that the relatively low nanosheet number in the coincubation system caused by the high molecular mass of MoS_2 may be one of important

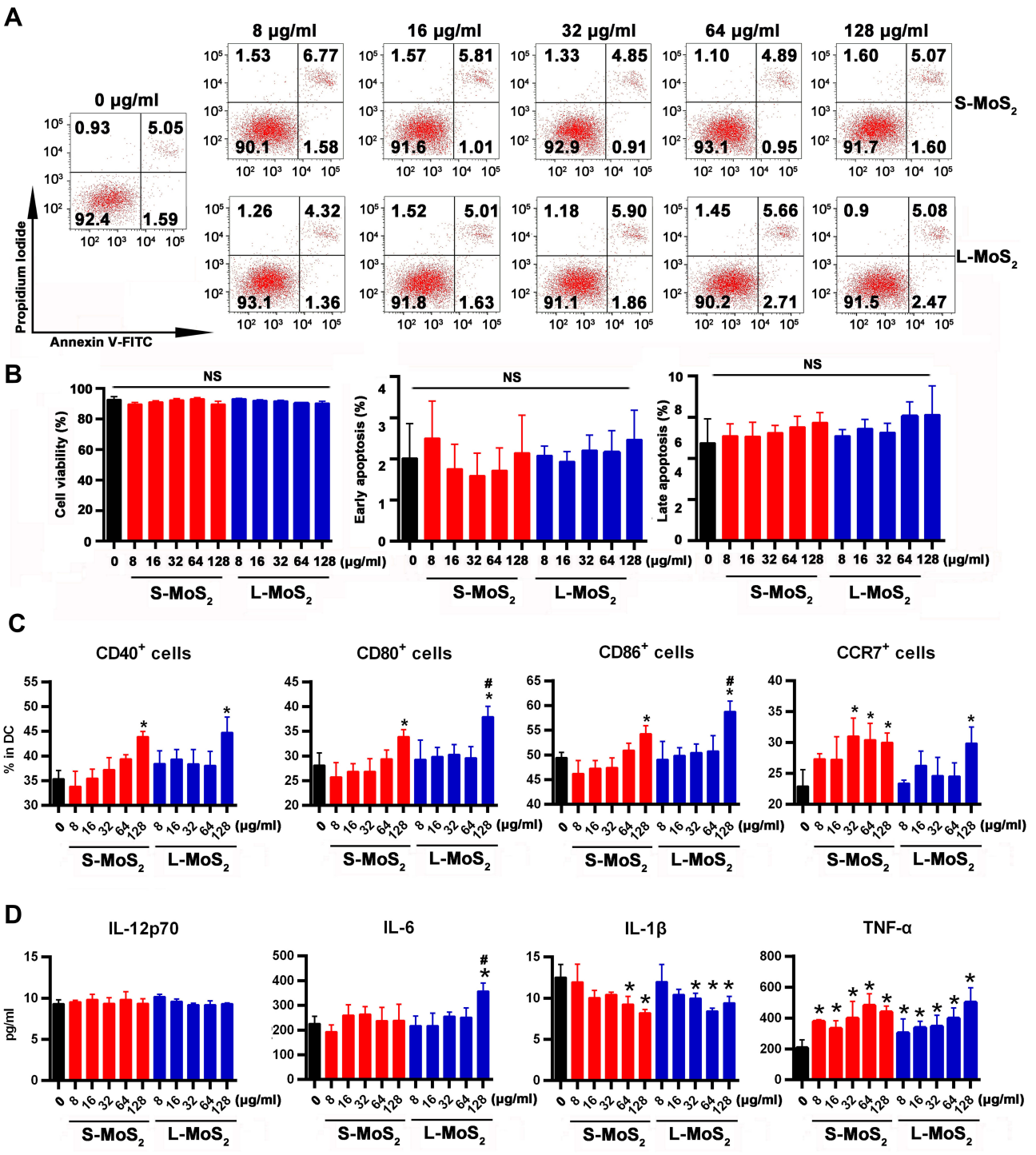

Figure 2 The dose effect of MSN treatment on the viability, surface markers and cytokine secretion of DCs.

Notes: (**A**) The viability of DCs was analyzed by combined staining with Annexin V-FITC and PI after being co-incubated with different doses of MSNs for 48 h. (**B**) Statistical data of the proportion of viability, early apoptosis and late apoptosis of DCs. (**C**) The expression of DC surface markers (CD40, CD80, CD86 and CCR7) was detected by flow cytometry. (**D**) ELISA was used to detect the secretion of IL-12p70, IL-6, IL-1β and TNF-α by DCs. *The difference was statistically significant ($p < 0.05$) compared with the control group. #The difference was statistically significant ($p < 0.05$) compared with the 128 μg/mL S-MoS_2 group.

Abbreviations: S-MoS_2, small MoS_2; L-MoS_2, large MoS_2; Annexin V-FITC, Annexin V-fluorescein isothiocyanate; NS, no statistical significance; MSNs, MoS_2 nanosheets; IL, interleukin; PI, propidium iodide; CD, cell differentiation; CCR7, chemokine C-C-Motif Receptor 7; DCs, dendritic cells; TNF-α, tumor necrosis factor; ELISA, enzyme-linked immunosorbent assay.

reasons. One supportive evidence was that only a small number of MSNs could be found inside DCs (Figure 1D). Furthermore, we doubled the incubation concentration of MSNs and detected the expression of CD80 and CCR7 (Figure S2), with a result demonstrating that improving the concentration of MSNs could further promote the maturation of DCs. For the comparison of the two sized MSNs, the overall tendency was consistent but a slightly stronger effect was detected with L-MSNs (higher CD80/86 expression and IL-6 secretion). In conclusion, those results highlight that MSNs have good biocompatibility and can dose-dependently improve the maturation of DCs.

MSNs Improve the Homing Ability of DCs

To examine whether MSN treatment would change the migration ability of DCs, we employed the confocal living cell tracking system to image the movement of individual cells ex vivo. After being incubated with MSNs for 48 h at 128 μg/mL, GFP^+ DCs were sequentially imaged for 12 h (Figure 3A and B). The data showed that MSN-pulsed DCs showed advantages in terms of the migration distance and velocity over the control DCs, demonstrating enhanced movement. There was no significant difference between the S-MSNs and L-MSNs.

Furthermore, we employed the footpad injection model combined with bioluminescence imaging to determine the in vivo lymphoid tissue homing ability of MSN-treated DCs. DCs derived from $Fluc^+$ transgenic mice were incubated with 128 μg/mL MSNs for 48 h, and then, the DCs were injected into the footpads of the recipient mice to test their capacity to drain to the popliteal lymph nodes (PLNs). The signal intensity (SI) was calculated by Living Image software. The migration rate was calculated as follows: SI (PLN)/SI (PLN + footpad). The sequentially detected data showed that at 4 h after injection, a small proportion of cells had migrated to the PLNs in the MSN-treated DCs, and the number of migrated cells gradually increased with time (Figure 3C). The statistical data in Figure 3D confirmed the imaging results, demonstrating that both S-MSNs and L-MSNs significantly promoted the local lymphoid homing ability of DCs, with an elevation fold of 2.2 ± 0.5 and 2.6 ± 0.6, respectively.

Under physiological conditions, tissue resident DCs need to leave non-lymphoid organs or tissues and migrate to the lymphatic or blood circulation before successfully entering the T cell region in the lymphoid tissues. DCs incubated with S-MSNs or L-MSNs for 48 h were further injected to recipient mice through the tail vein to mimic circulating DCs. We imaged the $Fluc^+$ DCs at 2 h after injection and the result showed that the distribution pattern of the DCs in each group was consistent: DCs were mainly distributed in the lung, with a small amount of them concentrated in the liver or spleen (Figure 3E). We then dissected the main organs and tissues of the mice at 48 h (Figure 3F). Results showed that most of the DCs in the control group were residual in the lungs. In contrast, DCs stimulated with S-MSNs and L-MSNs were more inclined to being located in the parapulmonary lymph nodes and liver lymph nodes, thus confirming the significantly enhanced lymphoid tissue homing ability of MSN-treated DCs.

Migration and homing are recognized as the two most remarkable characteristics of DCs, which makes them unique compared with other immune cells and directly determines their capacity to elicit T cells.[27,28] Previous studies have shown that for artificial vaccines, only less than 5% of the adoptive antigen-bearing DCs were capable of homing to the T cell region, making it the main reason why vaccines fail.[29–31] Immunologists have long tried to improve the migratory ability of DCs by directly targeting them or developing new vaccine adjuvants. One of our previous works proved the feasibility of using CpG-conjugated gold nanoparticles as an adjuvant to improve the homing ability of DCs.[32] Furthermore, we also found that naked AuNPs promoted the homing ability of DCs, which inspired us to focus on the immunoregulatory role of the nanoparticles themselves. The naked MSNs used in this study, ranging from 100 to 500 nm, could improve the homing ratio of DCs from 7.2 ± 2.8% to 18.8 ± 3.4%, and we speculate that the increased intensity could be further improved if the MSNs were designed as nano-carriers with conjugated TLR activators, such as CpG oligos.

ROS-Induced Cytoskeleton Arrangement Participates in the Improved Homing Ability of MSN-Treated DCs

Microfilaments and microtubules are important components of the cytoskeleton. They form the network structure of the intracellular skeleton and are responsible for cell migration.[33–35] To determine whether cytoskeleton organization was affected by MSN treatment, we visualized the organization of the microfilaments and microtubules by immunofluorescence staining (Figure 4A). In control DCs, the organization of both actin and tubulin showed typical low migratory characteristics: weak staining intensity, short false feet, and inconspicuous dendrites. However, MSN-treated DCs had more obvious dendrites and

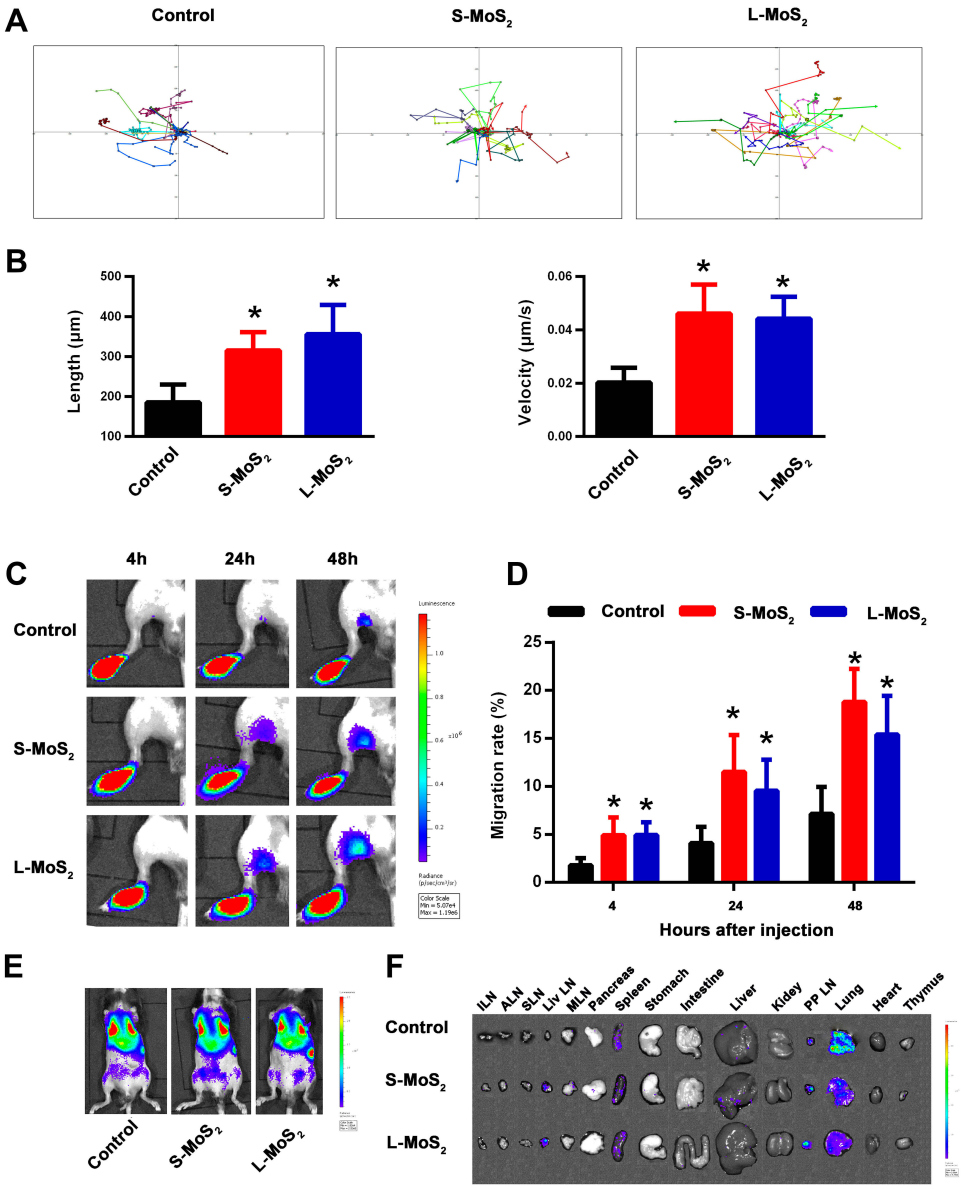

Figure 3 MSNs improved the ex vivo movement and in vivo homing ability of DCs.

Notes: (**A**) The ex vivo movement of DCs. After being incubated with MSNs for 48 h at 128 μg/mL, the movement of individual GFP^+ DCs was tracked by the confocal living cell tracking system. (**B**) Statistical data of the length and velocity of DC movement. (**C**) The in vivo homing of tissue resident DCs. A total of 1×10^6 DCs derived from L2G85.C57BL/6J mice were injected into the footpads of mice, and the in vivo migration to the PLNs was visualized at 4, 24 and 48 h by bioluminescence imaging. (**D**) Statistical data of the homing percentage. N = 5 for each group. (**E**) Imaging of the overall distribution of i.v. injected $Fluc^+$ DCs at 2 h. (**F**) The tissue accumulation of circulating DCs at 48 h after injection. A representative dataset from two or three replicates is shown. *$p < 0.05$ compared with the control group.

Abbreviations: S-MoS_2, small MoS_2; L-MoS_2, large MoS_2; ILN, inguinal lymph node; ALN, axillary lymph node; SLN, submaxillary lymph node; Liv LN, liver lymph node; MLN, mesenteric lymph node; PP LN, para-pulmonary lymph node; DCs, dendritic cells; MSNs, MoS_2 nanosheets; i.v., intravenous injection; GFP, green fluorescent protein; PLN, lymph node; Fluc, firefly luciferase.

stronger staining. In addition, the average fluorescence intensity of the microtubules and microfilaments was further calculated (Figure 4B), which confirmed the observations in Figure 4A and demonstrated that MSNs promoted the rearrangement of the DC cytoskeleton.

To explore the molecular mechanism by which MSNs promote the organization of cytoskeletons and to examine whether ROS participated in this process, DCFH-DA probes were used to visualize ROS accumulation in the DCs. Figure 4C showed that MSN treatment significantly upregulated ROS production, with no obvious difference observed between the S-MSN and L-MSN groups, which was further confirmed by the statistical data, as shown in Figure 4D. To investigate whether ROS production is related to cytoskeleton organization, N-acetylcysteine (NAC) was used as an antioxidant to prevent ROS

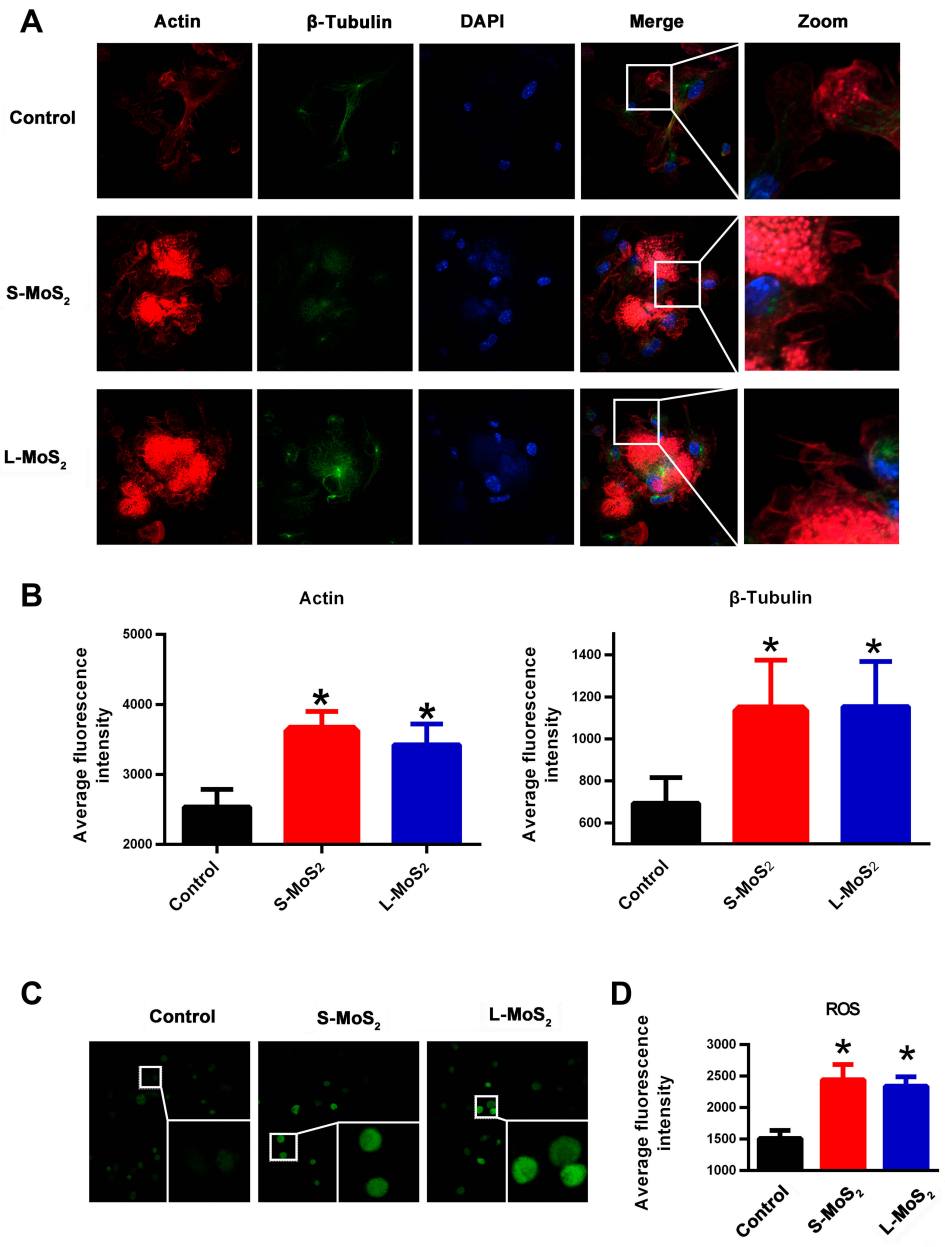

Figure 4 The cytoskeleton arrangement and ROS production of MSN-treated DCs.

Notes: (**A**) The organization of microfilaments and microtubules in DCs was respectively visualized by phalloidin and anti-β-tubulin. (**B**) Statistical data of the average fluorescence intensity of actin and tubulin staining. (**C**) ROS production in DCs at 48 h after MSN co-incubation, as detected by the DCFH-DA probe. (**D**) Statistical data of the average fluorescence intensity of ROS. A representative dataset from two or three replicates is shown. *$p < 0.05$ compared with the control group.

Abbreviations: S-MoS_2, small MSNs; L-MoS_2, large MSNs; DAPI, 4′,6-diamidino-2-phenylindole; DCs, dendritic cells; ROS, reactive oxygen species; MSNs, MoS_2 nanosheets; DCFH-DA, fluorescent probe 2, 7-dichlorofluorescein.

accumulation. As shown in Figure 5A and B, NAC pre-treatment did significantly interrupt the well-organized microfilaments in the MSN-treated DCs. Furthermore, the homing percentage of DCs was also significantly hindered by NAC treatment (Figure 5C and D).

Collectively, the above results support the conclusion that MSNs upregulate ROS generation in DCs, further promoting cytoskeletal rearrangement, and finally enhancing the migration ability of DCs. For nanomaterials, ROS are no doubt the most critical mediators for initiating toxicological effects by direct or indirect pathways. It has been demonstrated that direct ROS can be generated on the surface of NPs via electron—hole pair generation, chemical dissolution or the release of toxic metal ions.[36] On the other hand, NP exposure can also induce ROS generation by cells in a cumulative way, eliciting significant cell changes in terms of cellular

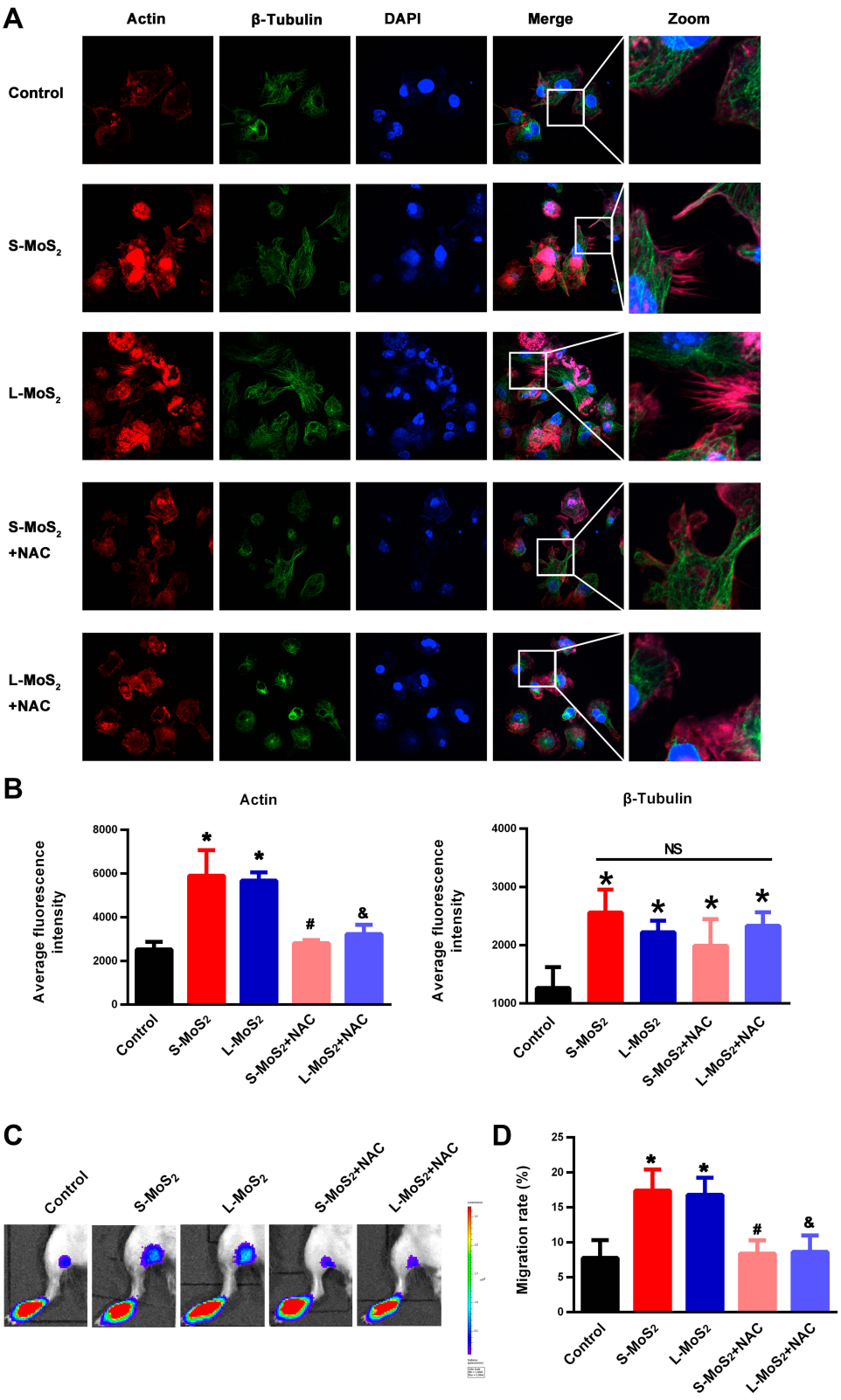

Figure 5 MSN-induced ROS elevation participated in the cytoskeleton arrangement and in vivo homing of DCs.

Notes: (**A**) The effect of NAC treatment on the organization of microfilaments and microtubules in MSN-treated DCs. (**B**) Statistical data of the average fluorescence intensity of actin and tubulin staining. (**C**) The effect of NAC treatment on the PLN homing of MSN-treated DCs. (**D**) Statistical data of the homing percentage. A representative dataset from two or three replicates is shown. N = 5 for each group. $^{*}p < 0.05$ compared with the control group. $^{\#}P < 0.05$ compared with the S-MoS_2 group. $\&p < 0.05$ compared with the L-MoS_2 group.

Abbreviations: S-MoS_2, small MoS_2; L-MoS_2, large MoS_2; DAPI, 4′,6-diamidino-2-phenylindole; NAC, N-acetyl-L-cysteine; DCs, dendritic cells; ROS, reactive oxygen species; MSN, MoS_2 nanosheet; NS, no statistical significance; PLN, lymph node.

morphology, metabolism and even DNA integrity when reaching a certain value of accumulation. Actually, whether MSN exposure induces ROS production is still a controversial topic. Yu et al demonstrated that chitosan functionalized MSNs induced ROS accumulation in human dermal cells[37] and in the gills and liver of adult zebrafish.[38] Consistently, Pardo et al[39] found that fullerene-like MSNs could induce robust protective antioxidant/detoxification defenses in human bronchial cells, indicating ROS generation in this cell line. Using *E. coli* as the model organism, Wu et al[40] and Qureshi et al[41] proved that the MSN exposure at a concentration of 100–1000 μg/mL dramatically increased the intracellular concentrations of ROS in bacteria. In contrast to the above findings, Zhang et al[42] proved that ultra-small (sub-5nm) cysteine-protected MSN dots played an antioxidative role via rapid reactions with O_2- and H_2O_2. Similarly, in another study, MSNs were used as a nano-enzymatic antioxidant with superior performance to scavenge free radicals.[43] We speculate that the differences in size, shape, surface chemistry and discrepancy in the experiment systems are the main reasons for the divergent or even totally controversial findings in these studies. Normally, ROS accumulation is recognized to be harmful because of the induced DNA damage and metabolic disorder.[44,45] Instead, findings in this study showed that MSN-induced ROS were favorable for the cytoskeleton organization and homing of DCs. We suggest that moderate ROS production resulting from mild interactions between MSNs and DCs is the most critical cause.

MSNs Promote the in vivo T Cell Priming Ability of DCs

Activating T cells is the ultimate mission of DCs. From the improved maturation and homing of DCs, enhanced T cell activation can be expected. To determine whether this effect is realized, DCs incubated with S-MSNs or L-MSNs were injected into the footpads of mice successively on day 1 and day 7. PLNs were taken on day 14 to evaluate the adaptive immune response against antigens from FBS in culture medium. This process is summarized in Figure 6A. The size of the PLNs that preliminarily reflects the intensity of the immune response are presented in Figure 6B. The results showed that PLNs from MSN-DC immunized mice were significantly larger than those of the control group, and no obvious difference was observed between the S-MSN- and L-MSN-treated groups. The absolute cell number of $CD4^+$ T helper, $CD8^+$ cytotoxic T lymphocytes and $B220^+$ B lymphocytes was further counted (Figure 6C). A consistent tendency was observed in the size of the PLNs, where the amount of all detected cell subtypes was higher in the MSN-treated group. Furthermore, the activation markers CD69, CD107a and ICOS on $CD4^+$ T cells (Figure 6D) and $CD8^+$ T cells (Figure 6E) as well as the intracellular cytokines (TNF-α and IFN-γ) of $CD8^+$ T cells (Figure 6F) were also significantly higher in the MSN-DC vaccinated mice. These results indicate that in the range of 100–500 nm, MSNs can improve the T cell priming ability of DCs independent of size, resulting in an enhanced downstream immune response of both $CD8^+$ cytotoxic T and B lymphocyte cells.

Many studies have reported that smaller nanomaterials can more easily enter cells, which can influence cell morphology, gene expression and cell proliferation by inducing the upregulation of certain genes.[46–48] In our work, S-MSNs and L-MSNs were not significantly different in terms of their ability to promote DC maturation, migration, and eventual activation. This indicates that in the range of 100–500 nm, the recognition, endocytosis and intracellular processing of MSNs by DCs are likely to be consistent, resulting in a consistent effect on DCs. These findings also suggest that MSNs of 100–500 nm are safe and within the optional range for the development of DC adjuvants.

For DC immunotherapy, cytokine-cocktail composed of 1000 U/mL IL-1β, 1000 U/IL-6, 1000 U/TNF-α and 1μg/mL PGE2 is the mostly used adjuvant. We selected several key indexes to compare the immune stimulatory capacity of MSNs with the existing adjuvants. Firstly, we examined the T cell priming ability of DCs stimulated with L-MSNs and cytokine-cocktail, respectively. Mice was vaccinated following the schematic diagram in Figure 6A and the intracellular synthesis of IFN-γ and TNF-α in $CD8^+$ T cells was detected (Figure S3A). Compared to control group, both of cytokine-cocktail and MSNs could improve the intensity of $CD8^+$ T activation. Furthermore, the number of IFN-γ^+ and TNF-α^+ T cells in L-MoS_2 group far exceeded that in cytokine-cocktail adjuvanted group. We further compared the expression of CD80 (a representative of allostimulatory markers, Figure S3Ba), CCR7 (Figure S3Bb), antigen presentation (Figures S3Bc and S3C) and the in vivo homing ability of DCs (Figure S3D) in those two groups. From those data, we acquired that the cytokine-cocktail had an advantage in upregulating the expression of allostimulatory markers. But the antigen presentation and LN-homing of cytokine-cocktail adjuvanted DCs were significantly lower than MSN-treated ones, which may be major causes for the relatively lower T cell priming capacity. This result was consistent with previous reports that only less than 5% of cytokine-cocktail stimulated DCs were capable of

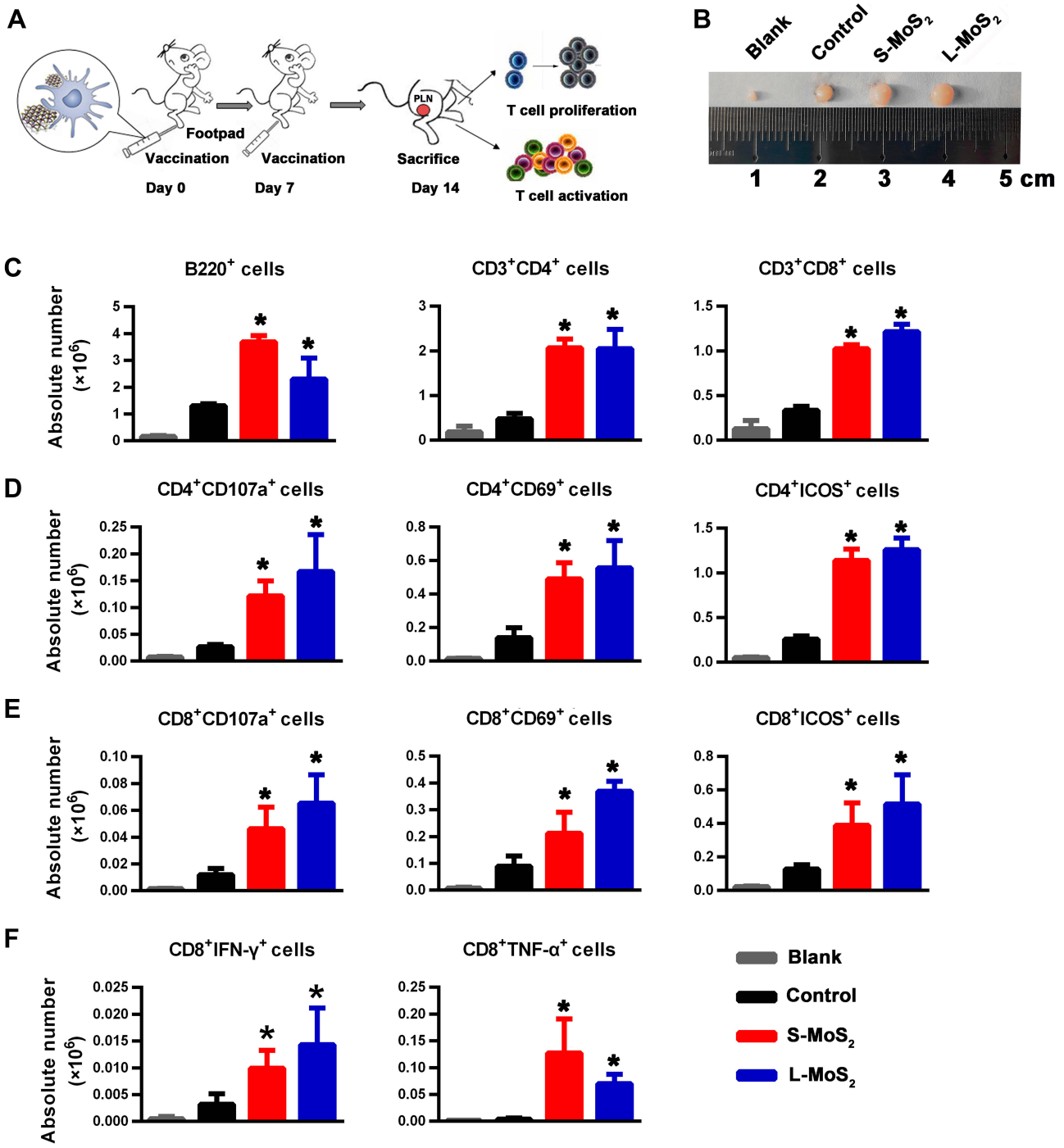

Figure 6 T cell immune response after footpad inoculation of DCs.

Notes: (**A**) Schematic diagram of the vaccination process. (**B**) The size of the PLNs from the DC-injected mice. The control group was injected with untreated DCs. Mice in the blank group did not receive DC infusion. (**C**) Absolute number of $B220^+$ cells, $CD4^+$ T cells and $CD8^+$ T cells in the PLNs. (**D**) Absolute number of $CD107a^+$ $CD4^+$ T cells, $CD69^+$ $CD4^+$ T cells and $ICOS^+$ $CD4^+$ T cells in the PLNs. (**E**) Absolute number of $CD107a^+$ $CD8^+$ T cells, $CD69^+CD8^+$ T cells, and $ICOS^+$ $CD8^+$ T cells in the PLNs. (**F**) Absolute number of IFN-γ^+ $CD8^+$ T cells and TNF-α^+ $CD8^+$ T cells in the PLNs. A representative dataset from two or three replicates is shown. N = 5 for each group. *$p < 0.05$ compared with the control group.

Abbreviations: S-MoS_2, small MoS_2; L-MoS_2, large MoS_2; DCs, dendritic cells; PLNs, popliteal lymph nodes; IFN-γ, interferon-γ; TNF-α, tumor necrosis factor-α; CD, cell differentiation; ICOS, inducible co-stimulator.

homing to the T cell region.[30–32] Also, investigations from others and our own indicated that the protein-enrichment capacity shared by most nanomaterials promoted antigen presentation by an intracellular antigen delivery way.[32,49,50]

Collectively, MSNs adjuvanted DCs are capable of activating T cells at a high efficiency. In addition, MSNs have an obvious advantage over cytokine-cocktails in promoting DC homing and antigen presentation.

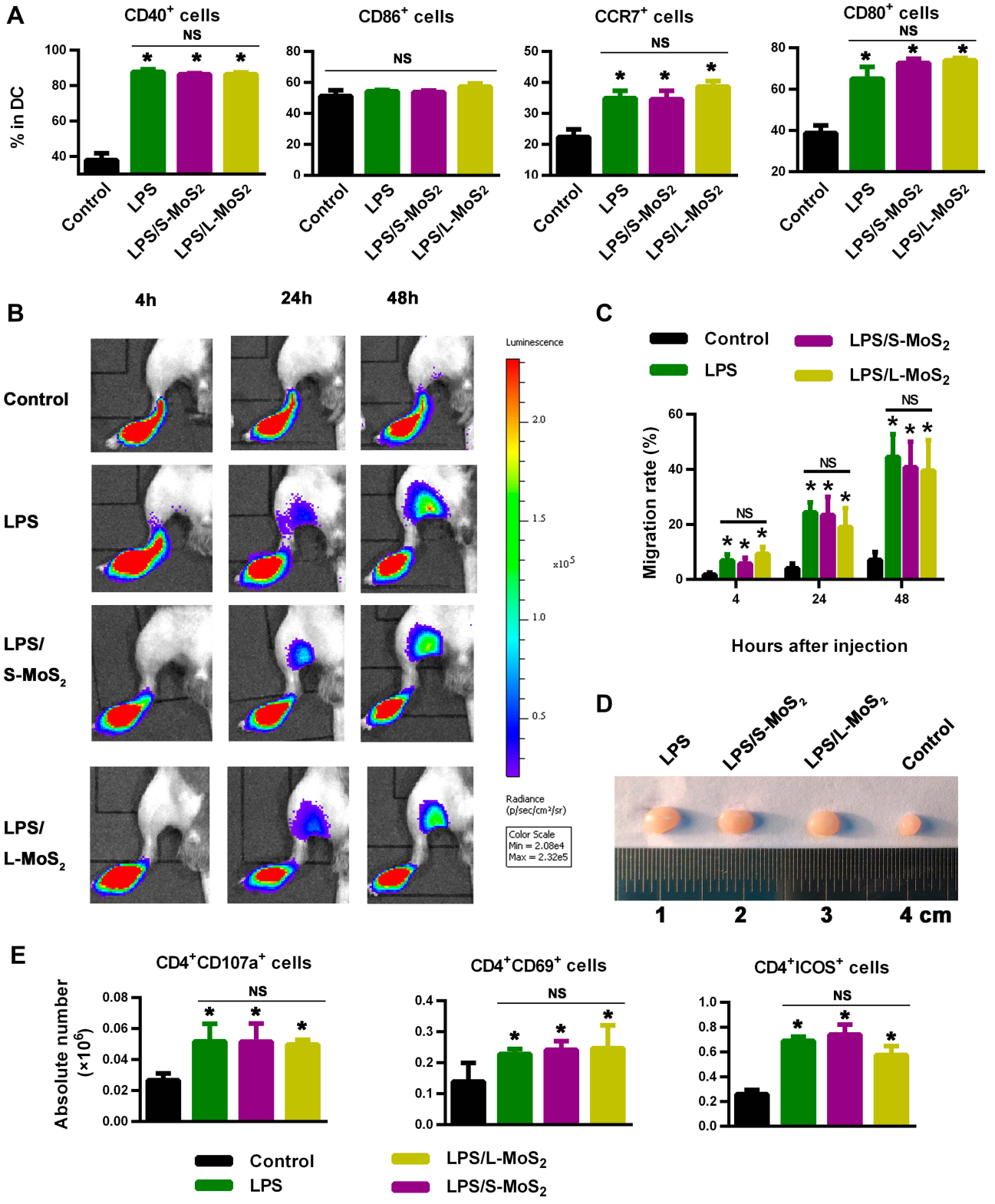

Figure 7 MSN treatment did not affect the response of DCs to LPS stimulation.

Notes: (**A**) Expression of DC surface markers, as detected by flow cytometry. (**B**) The PLN-homing ability of DCs, as detected by bioluminescence imaging. (**C**) Statistical data of the homing percentage. (**D**) The size of the PLNs from DC-immunized mice. (**E**) Absolute number of $CD107a^+$ $CD4^+$ T cells, $CD69^+$ $CD4^+$ T cells and $ICOS^+$ $CD4^+$ T cells in the PLNs of vaccinated mice. A representative dataset from two or three replicates is shown. N = 5–6 for each group. *$p < 0.05$ compared with the control group.

Abbreviations: S-MoS_2, small MoS_2; L-MoS_2, large MoS_2; DCs, dendritic cells; LPS, lipopolysaccharide, PLN, popliteal lymph node; MSN, MoS_2 nanosheet; NS, no statistical significance; CD, cell differentiation; CCR7, chemokine C-C-Motif Receptor 7; ICOS, inducible co-stimulator.

MSN Treatment Does Not Affect the Response of DCs to LPS Stimulation

For nano-vaccine development, being compatible with the naturally occurring immune response is a prerequisite for in vivo application, and this characteristic is even more important than its efficiency. Under physiological conditions, the most frequently occurring invasions are from bacteria and viruses, which causes strong immunogenic components (LPS, CpG, etc.) to be exerted on the TLRs of DCs and promotes the cascade amplification of the immune response.[51] We introduced LPS (100 ng/mL) into the MSN-DC co-incubation system to mimic pathogen invasion, and further analyzed DC changes. Figure 7A shows that adding LPS strongly stimulated the expression of CD40, CD80, CD86 and CCR7 on DCs, and neither S-MSNs nor L-MSNs had any affect the elevation of these allostimulatory molecules. Furthermore, a consistent tendency was observed in the DC in vivo homing evaluation (Figure 7B and C). Finally, following the same immune procedure in Figure 6A, mice were immunized by different combinations of LPS and MSNs to analyze the activated immune response. The PLNs of the LPS, "LPS + S-MSNs" and "LPS + L-MSNs" groups were significantly larger than those of the control group, and no differences were detected among these three groups (Figure 7D). The activation markers CD107a, CD69 and ICOS on $CD4^+$ T cells in the PLNs were further analyzed, and similar results were obtained (Figure 7E).

Collectively, from the above results, we conclude that exposure to MSNs, both S-MSNs and L-MSNs, had no effect on LPS-induced DC activation, homing and T cell priming. The good immuno-compatibility of MSNs provides supportive evidence for the feasibility of using them as vaccine adjuvants. Our findings also partially alleviate the concerns about interrupting the normal immune defenses by MSN exposure when they are designed for use as drug carriers or tissue engineering scaffolds. However, considering the enhancement of immature DC function by MSNs, MSNs should be cautiously applied in those suffering from chronic immune diseases (rheumatism, systemic lupus erythematosus, etc.), as the non-specific improvement in the immune response against auto-antigens may be detrimental to disease control.

Conclusion

Few-layered 100- to 500-nm MSNs were used in our study and showed little direct cytotoxicity to DCs. At a relatively higher dose (128 μg/mL), MSNs could size-independently improve the ex vivo maturation and lymphoid homing ability of DCs, and they had a considerably higher ability to elicit stronger $CD4^+$ and $CD8^+$ T cell immune responses. Furthermore, ROS-induced cytoskeleton arrangement participated in the improvement of the DC homing ability by MSNs. Finally, MSN exposure did not interrupt LPS-induced DC activation, homing and T cell priming. As the first work to systematically explore the immunoregulatory properties of MSNs, our findings provide evidence to broaden the application of MSNs as vaccine adjuvants and shed light on the immune risk assessment of in vivo administered nano-drugs. Of note, there are still important issues remain to be addressed. Firstly, a lot of work focusing dose optimization is required to maximize induced immune responses while with acceptable side effects. Second, there is still a need for systematically investigating the biodistribution and elimination from the organism of in vivo administered MSNs and their possible long-term toxicity to the recipients.

Acknowledgments

This work was supported by grants from the Mega-Project of Science Research (2017ZX10304402-003-004), the National Natural Science Foundation of China (81701583, 81770196, 81903624, 81970166) and the Foundation of 17QNP038.

Disclosure

The authors report no conflicts of interest in this work.

References

1. Novoselov KS, Geim AK, Morozov SV, et al. Electric field effect in atomically thin carbon films. *Science*. 2004;306(5696):666–669. doi:10.1126/science.1102896
2. Yang G, Zhu C, Du D, Zhu J, Lin Y. Graphene-like two-dimensional layered nanomaterials: applications in biosensors and nanomedicine. *Nanoscale*. 2015;7(34):14217–14231. doi:10.1039/C5NR03398E
3. Li L, Guo Z, Wang S, Li D, Yang X. Facile synthesis of MoS_2 quantum dots as fluorescent probes for sensing of hydroquinone and bioimaging. *Anal Methods*. 2019;11(26):3273–3364.
4. Gao L, Li Q, Deng Z, et al. Highly sensitive protein detection via covalently linked aptamer to MoS_2 and exonuclease-assisted amplification strategy. *Int J Nanomedicine*. 2017;12:7847–7853. doi:10.2147/IJN.S145585
5. Oudeng G, Au M, Shi J, Wen C, Yang M. One-step in situ detection of miRNA-21 expression in single cancer cells based on biofunctionalized MoS2 nanosheets. *ACS Appl Mater Interfaces*. 2018;10(1):350–360. doi:10.1021/acsami.7b18102
6. Jia L, Ding L, Tian J, et al. Aptamer loaded MoS2 nanoplates as nanoprobes for detection of intracellular ATP and controllable photodynamic therapy. *Nanoscale*. 2015;7(38):15953–15961. doi:10.1039/C5NR02224J
7. Chou SS, Kaehr B, Kim J, et al. Chemically exfoliated MoS_2 as near-infrared photothermal agents. *Angew Chem Int Ed Engl*. 2013;52(15):4160–4164. doi:10.1002/anie.201209229
8. Chen L, Zhou X, Nie W, et al. Marriage of albumin-gadolinium complexes and MoS2 nanoflakes as cancer theranostics for dual-modality magnetic resonance/photoacoustic imaging and photothermal therapy. *ACS Appl Mater Interfaces*. 2017;9(21):17786–17798. doi:10.1021/acsami.7b04488

9. Han J, Xia H, Wu Y, et al. Single-layer MoS2 nanosheet grafted upconversion nanoparticles for near-infrared fluorescence imaging-guided deep tissue cancer phototherapy. *Nanoscale*. 2016;8(15):7861–7865. doi:10.1039/C6NR00150E
10. Yin W, Yan L, Yu J, et al. High-throughput synthesis of single-layer MoS_2 nanosheets as a near-infrared photothermal-triggered drug delivery for effective cancer therapy. *ACS Nano*. 2014;8(7):6922–6933. doi:10.1021/nn501647j
11. Liu J, Li F, Zheng J, Li B, Zhang D, Jia L. Redox/NIR dual-responsive MoS2 for synergetic chemo-photothermal therapy of cancer. *J Nanobiotechnology*. 2019;17(1):78. doi:10.1186/s12951-019-0510-2
12. Zhang C, Zhang D, Liu J, et al. Functionalized MoS2-erlotinib produces hyperthermia under NIR. *J Nanobiotechnology*. 2019;17(1):76. doi:10.1186/s12951-019-0508-9
13. Sim H, Lee J, Park B, et al. High-concentration dispersions of exfoliated MoS_2 sheets stabilized by freeze-dried silk fibroin powder. *Nano Res*. 2016;9(6):1709–1722. doi:10.1007/s12274-016-1065-2
14. Blanco P, Palucka AK, Pascual V, Banchereau J. Dendritic cells and cytokines in human inflammatory and autoimmune diseases. *Cytokine Growth Factor Rev*. 2008;19(1):41–52. doi:10.1016/j.cytogfr.2007.10.004
15. Gunzer M, Janich S, Varga G, Grabbe S. Dendritic cells and tumor immunity. *Semin Immunol*. 2001;13(5):291–302. doi:10.1006/smim.2001.0325
16. Hussain S, Vanoirbeek JA, Hoet PH. Interactions of nanomaterials with the immune system. *Wiley Interdiscip Rev Nanomed Nanobiotechnol*. 2012;4(2):169–183. doi:10.1002/wnan.166
17. Jang J, Lim DH, Choi IH. The impact of nanomaterials in immune system. *Immune Netw*. 2010;10(3):85–91. doi:10.4110/in.2010.10.3.85
18. Smith MJ, Brown JM, Zamboni WC, Walker NJ. From immunotoxicity to nanotherapy: the effects of nanomaterials on the immune system. *Toxicol Sci*. 2014;138(2):249–255. doi:10.1093/toxsci/kfu005
19. Kitajima T, Caceres-Dittmar G, Tapia FJ, Jester J, Bergstresser PR, Takashima A. T cell-mediated terminal maturation of dendritic cells: loss of adhesive and phagocytotic capacities. *J Immunol*. 1996;157(6):2340–2347.
20. Caux C, Massacrier C, Vanbervliet B, et al. Activation of human dendritic cells through CD40 cross-linking. *J Exp Med*. 1994;180(4):1263–1272. doi:10.1084/jem.180.4.1263
21. Balanescu A, Radu E, Nat R, et al. Co-stimulatory and adhesion molecules of dendritic cells in rheumatoid arthritis. *J Cell Mol Med*. 2002;6(3):415–425. doi:10.1111/j.1582-4934.2002.tb00520.x
22. Michelsen KS, Aicher A, Mohaupt M, et al. The role of toll-like receptors (TLRs) in bacteria-induced maturation of murine dendritic cells (DCs). Peptidoglycan and lipoteichoic acid are inducers of DC maturation and require TLR2. *J Biol Chem*. 2001;276(28):25680–25686. doi:10.1074/jbc.M011615200
23. Lutz MB, Schuler G. Immature, semi-mature and fully mature dendritic cells: which signals induce tolerance or immunity? *Trends Immunol*. 2002;23(9):445–449. doi:10.1016/S1471-4906(02)02281-0
24. Wei ZT, Chng ELK, Sofer Z, Pumera M. Cytotoxicity of exfoliated transition-metal dichalcogenides (MoS_2, WS_2, and WSe_2) is lower than that of graphene and its analogues. *Chemistry*. 2014;20(31):9627–9632. doi:10.1002/chem.201402680
25. Appel JH, Li D, Podlevsky JD, et al. Low cytotoxicity and genotoxicity of two-dimensional MoS_2 and WS_2. *ACS Biomater*. 2016;2(3):361–367. doi:10.1021/acsbiomaterials.5b00467
26. Li X, Gong Y, Zhou X, et al. Facile synthesis of soybean phospholipid-encapsulated MoS_2 nanosheets for efficient in vitro and in vivo photothermal regression of breast tumor. *Int J Nanomedicine*. 2016;11:1819–1833. doi:10.2147/IJN.S104198
27. Austyn JM, Kupiec-Weglinski JW, Hankins DF, Morris PJ. Migration patterns of dendritic cells in the mouse. Homing to T cell-dependent areas of spleen, and binding within marginal zone. *J Exp Med*. 1988;167(2):646–651. doi:10.1084/jem.167.2.646
28. Alvarez D, Vollmann EH, von Andrian UH. Mechanisms and consequences of dendritic cell migration. *Immunity*. 2008;29(3):325–342. doi:10.1016/j.immuni.2008.08.006
29. O'Neill DW, Adams S, Bhardwaj N. Manipulating dendritic cell biology for the active immunotherapy of cancer. *Blood*. 2004;104(8):2235–2246. doi:10.1182/blood-2003-12-4392
30. Morse MA, Coleman RE, Akabani G, Niehaus N, Coleman D, Lyerly HK. Migration of human dendritic cells after injection in patients with metastatic malignancies. *Cancer Res*. 1999;59(1):56–58.
31. Vries IJMD, Krooshoop DJEB, Scharenborg NM, Lesterhuis WJ, Figdor CG. Effective migration of antigen-pulsed dendritic cells to lymph nodes in melanoma patients is determined by their maturation state. *Cancer Res*. 2003;63(1):12–17.
32. Zhou Q, Zhang Y, Du J, et al. Different-sized gold nanoparticle activator/antigen increases dendritic cells accumulation in liver-draining lymph nodes and CD8+ T cell responses. *ACS Nano*. 2016;10(2):2678–2692. doi:10.1021/acsnano.5b07716
33. Ingber DE, Dike L, Hansen L, et al. Cellular tensegrity: exploring how mechanical changes in the cytoskeleton regulate cell growth, migration, and tissue pattern during morphogenesis. *Int Rev Cytol*. 1994;150:173–224.
34. Malech HL, Root RK, Gallin JI. Structural analysis of human neutrophil migration. Centriole, microtubule, and microfilament orientation and function during chemotaxis. *J Cell Biol*. 1977;75(3):666–693. doi:10.1083/jcb.75.3.666
35. Dogterom M, Koenderink GH. Actin–microtubule crosstalk in cell biology. *Nat Rev Mol Cell Biol*. 2019;20:38–54. doi:10.1038/s41580-018-0067-1
36. Nel A, Xia T, Meng H, et al. Nanomaterial toxicity testing in the 21st century: use of a predictive toxicological approach and high-throughput screening. *Acc Chem Res*. 2012;46(3):607–621. doi:10.1021/ar300022h
37. Yu Y, Wu N, Yi Y, et al. Dispersible MoS_2 nanosheets activated TGF-β/Smad pathway and perturbed the metabolome of human dermal fibroblasts. *ACS Biomater Sci Eng*. 2017;3(12):3261–3272. doi:10.1021/acsbiomaterials.7b00575
38. Yu Y, Yi Y, Li Y, et al. Dispersible MoS_2 micro-sheets induced a proinflammatory response and apoptosis in the gills and liver of adult zebrafish. *RSC Adv*. 2018;8(32):17826–17836. doi:10.1039/C8RA00922H
39. Pardo M, Shuster-Meiseles T, Levin-Zaidman S, Rudich A, Rudich Y. Low cytotoxicity of inorganic nanotubes and fullerene-like nanostructures in human bronchial epithelial cells: relation to inflammatory gene induction and antioxidant response. *Environ Sci Technol*. 2014;48(6):3457–3466. doi:10.1021/es500065z
40. Wu N, Yu Y, Li T, et al. Investigating the influence of MoS_2 nanosheets on E. coli from metabolomics level. *PLoS One*. 2016;11(12):e0167245. doi:10.1371/journal.pone.0167245
41. Qureshi N, Patil R, Shinde M, et al. Innovative biofilm inhibition and anti-microbial behavior of molybdenum sulfide nanostructures generated by microwave-assisted solvothermal route. *Appl Nanosci*. 2015;5(3):331–341. doi:10.1007/s13204-014-0322-5
42. Zhang XD, Zhang J, Wang J, et al. Highly catalytic nanodots with renal clearance for radiation protection. *ACS Nano*. 2016;10(4):4511–4519. doi:10.1021/acsnano.6b00321
43. Chen T, Zou H, Wu X, et al. Nanozymatic antioxidant system based on MoS_2 nanosheets. *ACS Appl Mater Interfaces*. 2018;10(15):12453–12462. doi:10.1021/acsami.8b01245
44. Richards SA, Muter J, Ritchie P, Lattanzi G, Hutchison CJ. The accumulation of un-repairable DNA damage in laminopathy progeria fibroblasts is caused by ROS generation and is prevented by treatment with N-acetyl cysteine. *Hum Mol Genet*. 2011;20(20):3997–4004. doi:10.1093/hmg/ddr327
45. Rodríguez-Vargas JM, Ruiz-Magaña MJ, Ruiz-Ruiz C, et al. ROS-induced DNA damage and PARP-1 are required for optimal induction of starvation-induced autophagy. *Cell Res*. 2012;22(7):1181–1198. doi:10.1038/cr.2012.70

46. Du J, Wang S, You H, Zhao X. Understanding the toxicity of carbon nanotubes in the environment is crucial to the control of nanomaterials in producing and processing and the assessment of health risk for human: a review. *Environ Toxicol Pharmacol*. 2013;36(2):451–462. doi:10.1016/j.etap.2013.05.007
47. Chithrani BD, Ghazani AA, Chan WCW. Determining the size and shape dependence of gold nanoparticle uptake into mammalian cells. *Nano lett*. 2006;6(4):662–668. doi:10.1021/nl052396o
48. Forte M, Iachetta G, Tussellino M, et al. Polystyrene nanoparticles internalization in human gastric adenocarcinoma cells. *Toxicol In Vitro*. 2016;31:126–136. doi:10.1016/j.tiv.2015.11.006
49. Molino NM, Anderson AK, Nelson EL, Wang SW. Biomimetic protein nanoparticles facilitate enhanced dendritic cell activation and cross-presentation. *ACS Nano*. 2013;7(11):9743–9752. doi:10.1021/nn403085w
50. Han JA, Kang YJ, Shin C, et al. Ferritin protein cage nanoparticles as versatile antigen delivery nanoplatforms for dendritic cell (DC)-based vaccine development. *Nanomedicine*. 2014;10(3):561–569. doi:10.1016/j.nano.2013.11.003
51. Raymond CR, Wilkie BN. Toll-like receptor, MHC II, B7 and cytokine expression by porcine monocytes and monocyte-derived dendritic cells in response to microbial pathogen-associated molecular patterns. *Vet Immunol Immunopathol*. 2005;107(3–4):235–247. doi:10.1016/j.vetimm.2005.05.008